Heliyon 10 (2024) e35975

Contents lists available at ScienceDirect

Heliyon

journal homepage: www.cell.com/heliyon

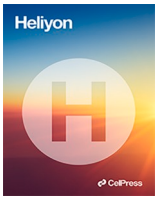

Research article

Comparison of potassium catalysts on zeolite sodium A and X in transesterification of palm oil and active species specification

Piyanat Seejandee [a], Nattawut Osakoo [b], Pakawan Sereerattanakorn [a], Panot Krukkratoke [a], Chalermpan Keawkumay [b], Chaianun Pansakdanon [a], Jatuporn Wittayakun [a,*], Narong Chanlek [c], Krittanun Deekamwong [b], Sanchai Prayoonpokarach [a,**]

[a] School of Chemistry, Institute of Science, Suranaree University of Technology, Nakhon Ratchasima, 30000, Thailand
[b] Institute of Research and Development, Suranaree University of Technology, Nakhon Ratchasima, 30000, Thailand
[c] Synchrotron Light Research Institute, Nakhon Ratchasima, 30000, Thailand

ARTICLE INFO

Keywords:
Potassium
Zeolite A
Zeolite X
Palm oil
Biodiesel
Transesterification

ABSTRACT

Heterogeneous catalysts consisting of potassium supported on zeolites are active for transesterification, but the effect of zeolite properties is not clearly understood. This work compares catalysts containing 12 wt.% potassium on zeolite sodium A and X (12K/NaA and 12K/NaX) in terms of performance and physicochemical properties. Both catalysts were prepared by ultrasound-assisted impregnation with potassium acetate buffer. 12K/NaA is a better catalyst in transesterification of palm oil, giving a higher biodiesel yield than 12K/NaX in the first run (99.1 ± 0.3 % and 77.9 ± 2.2 %, respectively). From characterization by CO_2-TPD, XRD, FTIR, XPS, and SEM-EDS, both catalysts have similar basicity but different dispersion of carbonates and interaction on the zeolites. The 12K/NaA has those species on external surfaces and more monodentate carbonate than 12K/NaX. Ion exchange occurs between potassium ions from the precursor and sodium ions from the zeolite. Moreover, 12K/NaA is more stable, providing higher biodiesel yields in the second and third catalytic cycles.

1. Introduction

Biodiesel or fatty acid methyl ester (FAME) is an alternative fuel produced by transesterification [1,2] of various vegetable oils [3–8] or animal fats [9] with methanol, and a blend of palm oil with animal fat [10]. Palm oil is one of the feedstocks that is not expensive and widely available in Southeast Asia [11]. In transesterification, either a homogeneous or heterogeneous catalyst is required, and the catalyst's basicity directly affects the biodiesel yield. Common homogeneous catalysts used in commercial and industrial biodiesel production include potassium hydroxide (KOH), sodium hydroxide (NaOH), and alkali bases [2]. However, the homogeneous process requires neutralization and washing, which produces a large amount of wastewater and is difficult to separate and reuse. Thus, heterogeneous catalysts are developed due to their simple separation and reusability [12,13]. Several heterogeneous catalysts have been developed including CaO on zeolite and silica [5,14], CaO from limescale source [15], BaO and MgO on zeolite

* Corresponding author.
** Corresponding author.
E-mail addresses: jatuporn@sut.ac.th (J. Wittayakun), sanchaip@sut.ac.th (S. Prayoonpokarach).

https://doi.org/10.1016/j.heliyon.2024.e35975
Received 29 July 2024; Received in revised form 6 August 2024; Accepted 7 August 2024
Available online 8 August 2024

ZSM-5 [16,17], CaFe on MOF [18], CaO/CBT [19], sodium aluminate [20], β-zeolite-supported sulfated metal oxide [21], CeO_2 functionalized on SBA-15 [22], and modified natural zeolite [23].

Zeolite LTA (NaA) and FAU (NaX) have been used as supports for heterogeneous catalysts. Both zeolite types have large surface areas, strong active sites, uniform porous structures, and high thermal stability [24,25]. They can be synthesized using a simple method and are widely used commercially. The NaA and NaX zeolites have similar Si/Al ratios (1.0 and 1.0–1.5, respectively) but different pore sizes (0.43 nm and 0.74 nm, respectively). Xie et al. [8] loaded 4–14 % KOH on zeolite NaX (KOH/NaX) for the transesterification of soybean oil. The zeolite structure was stable upon the catalyst preparation. However, the reaction took 8 h to get the highest conversion. In contrast, Trisupakitti et al. [26] prepared 1–4 % KOH/NaA with the same preparation method for transesterification of coconut oil. The zeolite structure and morphology changed after the catalyst preparation, suggesting that KOH might not be a good precursor. The biodiesel yield was around 60 % from the 4–6 h reaction time. According to the studies by Xie et al. [8] and Trisupakitti et al. [26] the potassium catalysts of NaX and NaA were tested separately on different oils and different conditions. Thus, the effect of zeolite type on transesterification and potassium precursor has not been studied under the same reaction conditions.

In terms of potassium precursors, NolHakim et al. [27] prepared the catalysts with potassium carbonate (K_2CO_3) and KOH on Al_2O_3. Both catalysts gave high yields in the first run, but the yield decreased in the following cycles. However, K_2CO_3/Al_2O_3 can be reused better than KOH/Al_2O_3. Foroutan et al. [28] employed banana-biochar/Fe_3O_4/ZIF-67@K_2CO_3 to produce biodiesel from waste cooking oil and proposed the reaction mechanism. Mawlid et al. [29] reported a clean approach to utilize K_2CO_3 on orange peel biochar as a catalyst for transesterification of waste frying oil. Thus, K_2CO_3 could be a promising active species for the transesterification of vegetable oil.

Potassium carbonate supported on zeolite X and Y has been prepared from the impregnation of potassium acetate buffer (CH_3COOK/CH_3COOH) followed by calcination [3,4,7]. NaX and NaY have the same FAU structure but a different Si/Al ratio, resulting in different basicity. NaX (Si/Al ratio of 1.0–1.5) has a higher basicity than NaY (Si/Al ratio >1.5). The buffer precursor can prevent the structure of NaY from collapsing [6]. The use of K/NaX as a catalyst using the same preparation method in the transesterification of Jatropha seed oil, K/NaX gave a higher biodiesel yield than K/NaY. Moreover, Rakmae et al. [3] improved the dispersion of potassium on K/NaY catalysts prepared with potassium acetate buffer by ultrasound-assisted impregnation. The better potassium dispersion of the catalyst improved the performance of K/NaY in the transesterification of palm oil.

Recently, Kosawatthanakun et al. [4] compared K/NaX and K/NaY prepared by ultrasound-assisted impregnation on the transesterification of palm oil. K/NaX was a better catalyst than K/NaY in terms of biodiesel yield and catalyst stability. However, the structure of both zeolites seems to collapse after the catalyst preparation, likely due to hydrolysis of Si–O–Al bonds in the presence of potassium species [30]. It has been known that the structure of zeolite X is not stable, for example, upon ion exchange and calcination [31]. Thus, zeolites with better stability should be investigated for further catalyst development.

The goal of this work is to further improve the zeolite-supported potassium catalyst for better performance. Zeolite X could be replaced by another zeolite with higher stability and basicity. We selected zeolite NaA as an alternative support because it has been reported to be stable over a wide range of testing conditions [32–34]. NaA has a lower Si/Al ratio and a smaller cavity size than NaX zeolites. This is the first report on the comparison of potassium catalysts on NaA (K/NaA) and NaX (K/NaX) in terms of catalytic performance in transesterification of palm oil and physicochemical properties from several characterization methods. In this work, K/NaA and K/NaX were prepared by ultrasound-assisted impregnation and tested in the transesterification of palm oil. The physicochemical properties of the catalysts were studied by carbon dioxide temperature-programmed desorption (CO_2-TPD), X-ray diffraction (XRD), Fourier transform infrared spectroscopy (FTIR), X-ray photoelectron spectroscopy (XPS), N_2 adsorption-desorption analysis, thermogravimetric analysis (TGA) and scanning electron microscopy with energy dispersive spectroscopy (SEM-EDS).

2. Experimental

2.1. Materials and chemicals

The commercial zeolites in sodium form, NaA and NaX, were purchased from Sigma Life Science and Sigma-Aldrich, respectively. The components in atomic percent from SEM-EDS were as follows: NaA, Al 12.38 %, Si 12.48 %, O 62.26 %, and Na 12.88 %, and NaX, Al 11.20 %, Si 16.27 %, O 59.90 %, and Na 12.63 %. Chemicals for catalyst preparation were potassium acetate (97.0 % CH_3COOK, ACS for analysis grade, Carlo Erba), glacial acetic acid (99.7 % CH_3COOH, AR grade, RCL Labscan), and deionized (DI) water. Chemicals for catalytic testing in transesterification were methyl alcohol (99.9 % CH_3OH, analytical grade, Carlo Erba), n-Hexane (96 % $CH_3(CH_2)_4CH_3$, HPLC-Isocratic grade, Carlo Erba) and palm oil (cooking oil, Olein brand). Chemicals for biodiesel yield determination by thin layer chromatography (TLC) were methyl nonadecanoate (C19 fatty acid methyl esters (FAME), Sigma-Aldrich, Switzerland), petroleum ether (AR grade, JT Baker), diethyl ether ($C_4H_{10}O$, AR grade, JT Baker) and glacial acetic acid (99.7 % CH_3COOH, AR grade, RCL Labscan). A certified standard mixture was Fatty Acid Methyl Ester Mix C8–C24 (CRM18918, Sigma-Aldrich, USA) and C19 (methyl nonadecanoate, $C_{19}(CH_3(CH_2)_{17}COOCH_3$, 98 %, Sigma-Aldrich) with a concentration 5 mg/mL in hexane was used as an internal standard. Air zero (20–22 % O_2 in N_2) for TGA was supplied by Linde (Thailand) Public Company Limited.

2.2. Catalyst preparation

The catalysts with 12 wt% of potassium were prepared by ultrasound-assisted impregnation of commercial zeolites NaA and NaX, as reported by Rakmae et al. [3]. Potassium acetate buffer solution (2.2 mL, pH 5.5) was dropped onto each support (2.0 g) in an

evaporation dish with stirring provided for 10 min and then sonicated for 10 min. The resulting mixture in the dish was covered with aluminium foil and dried at room temperature for 24 h and at 80 °C for another 24 h. Finally, the dried mixture was calcined at 500 °C for 3 h with a heating rate of 1 °C/min under static conditions. The obtained catalysts were named 12K/NaA and 12K/NaX.

2.3. Catalytic testing in transesterification

The performance of 12K/NaA and 12K/NaX in the transesterification of palm oil with methanol was adapted from Rakmae et al. [3]. The reaction was carried out in a batch reactor consisting of a 50-mL two-neck round bottom flask equipped with a water-cooled condenser with a thermometer. The catalyst powder (0.2 g) was mixed with methanol (3.7 mL) in the reactor, heated to 60 °C in a silicone oil bath, and stirred magnetically for 30 min. Then, palm oil (5.0 g) was added quickly to the mixture. After 3 h, the mixture was cooled to room temperature. The catalyst was separated by filtration with filter paper No.5. The excess methanol was removed by a rotary evaporator at 50 °C. The final mixture was transferred to a separatory funnel allowing a phase separation of biodiesel (top layer) and glycerol (bottom layer).

The top-layered product was analyzed preliminarily by thin layer chromatography (TLC), according to Manadee et al. [7] and Supamathanon et al. [6]. The stationary phase was silica gel, and the mobile phase was a solution containing petroleum ether, diethyl ether, and glacial acetic acid with 85:15:1 volume ratio. The types of fatty acid methyl esters (FAMEs) were analyzed by gas chromatography-mass spectrometry (GC-MS) by Agilent Technology, model 7890A MS triple quad according to the EN-14103 standard method. The biodiesel sample (50 mg) in a 1.5-mL vial was added with 1 mL of the C19 internal standard and the solution was filtered through a 0.22-μm filter. The GC-MS condition is shown in Table S1 in Supplementary Materials**.** The MS libraries were matched using the NIST MS Search Program 2.0 to define the FAME types. The probability-based matching algorithm was used to evaluate the mass spectra of the Agilent MS detector. The FAMEs were determined using gas chromatography-flame ionization detection (GC-FID) by Shimadzu model GC-14A FID/TCD. The sample was prepared according to the EN-14103 standard method. The condition of GC-FID is shown in Table S2 in Supplementary Materials. The FAMEs or biodiesel yield from GC-FID is calculated by equation (1) [35,36].

$$\text{Biodiesel Yield } (\%) = \frac{(\sum \text{A}) \; - \; \text{AEI}}{\text{AEI}} \times \frac{\text{CEI} \times \text{VEI}}{\text{m}} \; \times \; 100 \tag{1}$$

Where $\sum$A is the total peak area from the FAMEs C8 to C24, AEI is the peak area of an internal standard C19 FAME (IS C19), CEI is the concentration in mg/mL of IS C19, VEI is the volume in mL of IS C19 solution, and m is the mass in mg of the biodiesel sample.

The spent catalyst was regenerated by washing twice with 5 mL of methanol and twice with 10 mL of hexane and drying overnight in a hot air oven at 90 °C and tested in transesterification using a procedure similar to the fresh catalysts.

2.4. Catalyst characterizations

The basicity of the catalysts was determined by CO_2-TPD on a Belcat-B chemisorption analyzer, as described by Kosawatthanakun et al. [4]. The phases of parent zeolites and K catalysts were characterized by powder X-ray diffraction (XRD, Bruker D8 ADVANCE) with Cu K_a radiation operating at 40 kV. The 2θ scan range is 5 to 50°, with a step increment of 0.02. The functional groups of the zeolites and catalysts were confirmed by Fourier transform infrared spectroscopy (FTIR, Bruker model Tensor 27) in attenuated total reflectance (ATR) mode with a resolution of 4 cm^{-1}. The chemical surface-active species and the interaction of the active phase with zeolite support were characterized by X-ray photoelectron spectroscopy (XPS, ULVAC-PHI PHI 5000 Versa Probe II) with Al Kα radiation. The binding energy (BE) peaks were calibrated using the standard references of the C1s peak at 284.80 eV. The Multipak program was used to fit XPS peaks using a set of Gaussian values of 80 %, and the full width at half-maximum (FWHM) of the fitted peaks is in the range of 1.80 eV.

The morphology and elemental compositions of the zeolites and the catalysts were determined by using field emission scanning electron microscopy and energy dispersive x-ray spectrometer (FE-SEM-EDS, Zeiss AURIGA model JSM-7800F). The sample powder was dispersed on carbon tape on an aluminium stub and coated with carbon (FE-SEM) or gold (EDS) by sputtering (LEICA EM ACE600). The Si/Al ratio of the parent zeolites and the quantities of potassium, sodium, aluminum, and silicon were determined by an inductively coupled plasma optical emission spectrometer (ICP-OES, PerkinElmer, model optima 8000). Potassium in biodiesel and glycerol products was also determined by ICP-OES. The sample preparation procedures for ICP-OES analysis are in the Supplementary information.

3. Results and discussion

3.1. Catalytic testing in transesterification of palm oil

After the catalytic testing and methanol removal, the product has two layers. The top layer is biodiesel, and the bottom layer is glycerol. The biodiesel layers from 12K/NaA and 12K/NaX were analyzed by GC-FID and GC-MS. The chromatograms from the three reaction batches are similar. Examples of GC-FID chromatograms from the first batch are shown in Fig. 1a and b; they are similar to those in the literature [4]. The biodiesel yields from 12K/NaA and 12K/NaX are 99.1 ± 0.3 % and 77.9 ± 2.2 %, respectively. The results are consistent with TLC screening that 12K/NaA is the better catalyst (see Fig. S1 in Supplementary Materials). Trisupakitti

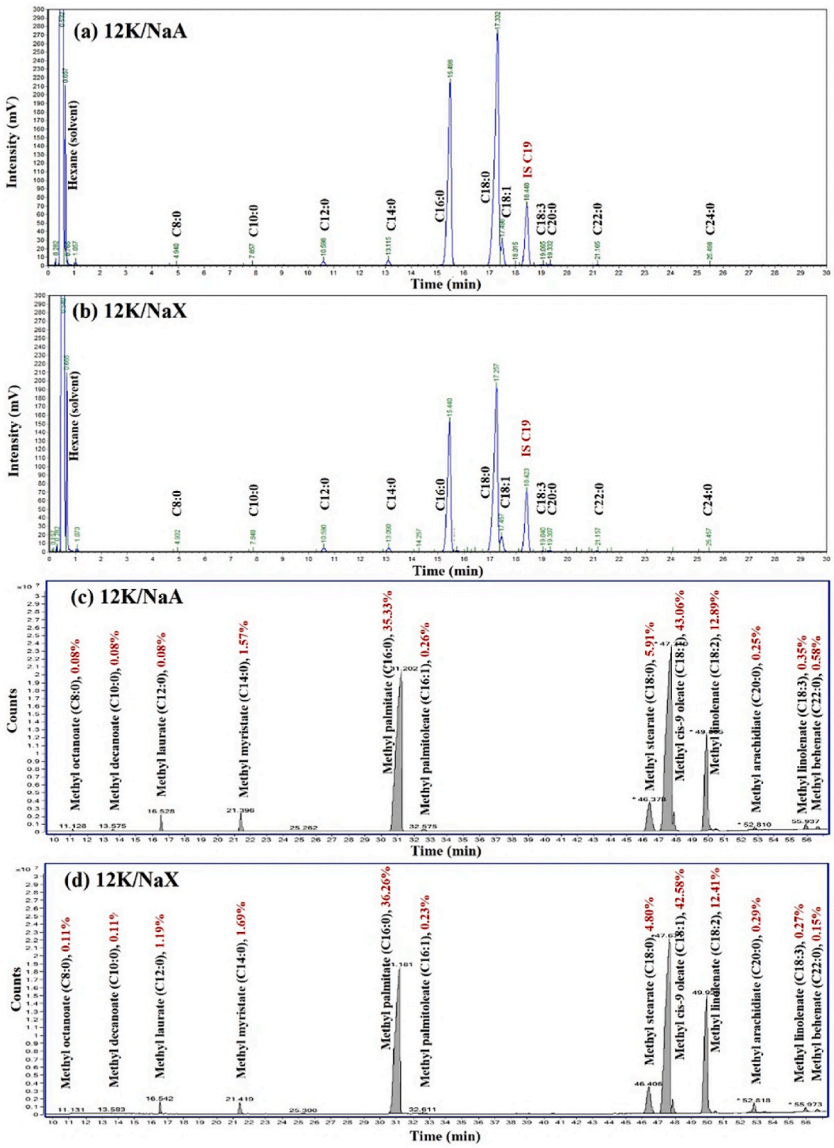

Fig. 1. Chromatograms of biodiesel products from transesterification of palm oil on 12K/NaA and 12K/NaX from the first reaction cycle (a,b) by GC-FID and (c,d) by GC-MS.

et al. [26] also reported that potassium catalysts from KOH on zeolite NaA were active for transesterification of coconut oil. From the chromatograms, the major components are C16 and C18. However, the separation of C16 and C18 was not clear due to the short column. Thus, the samples were further analyzed by GC-MS with a longer column. The GC-MS chromatograms of biodiesel products from 12K/NaA and 12K/NaX are shown in Fig. 1c and d, respectively. The major components were C18:1, followed by C16:0. Although both catalysts have the same potassium loading, they have different catalytic performances. Consequently, 12K/NaA and 12K/NaX catalysts were characterized extensively to determine parameters influencing the catalytic activity.

3.2. Characterization of as-prepared and calcined 12K/NaA and 12K/NaX catalysts

The CO_2-TPD profiles of the bare zeolite and catalysts are shown in Fig. 2. The desorption from the bare zeolites occurs at 100–500 °C. The total basic strength of NaA (0.683 mmol g^{-1}) is higher than NaX (0.366 mmol g^{-1}). NaA is more basic than NaX due to the higher Al content [37]. The TPD profiles of the calcined catalysts are significantly different from the parent zeolites. The profile could be divided into three temperature ranges. The first range, 100–300 °C, corresponds to a weak basic site. The second range, 300–550 °C, corresponds to a medium basic site. The last range, 550–800 °C, corresponds to a strong basic site. However, the peak temperature at 550–800 °C is due to the decomposition of K_2CO_3 to K_2O and CO_2 (g), as suggested by the TGA results. The similar

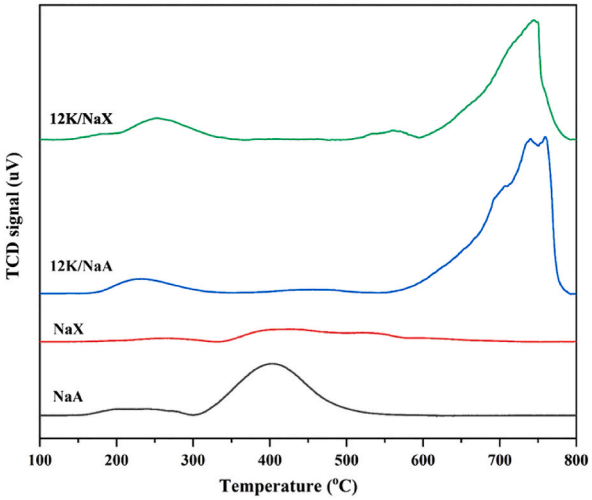

Fig. 2. CO_2-TPD profiles of bare zeolites and calcined 12K/NaA and 12K/NaX.

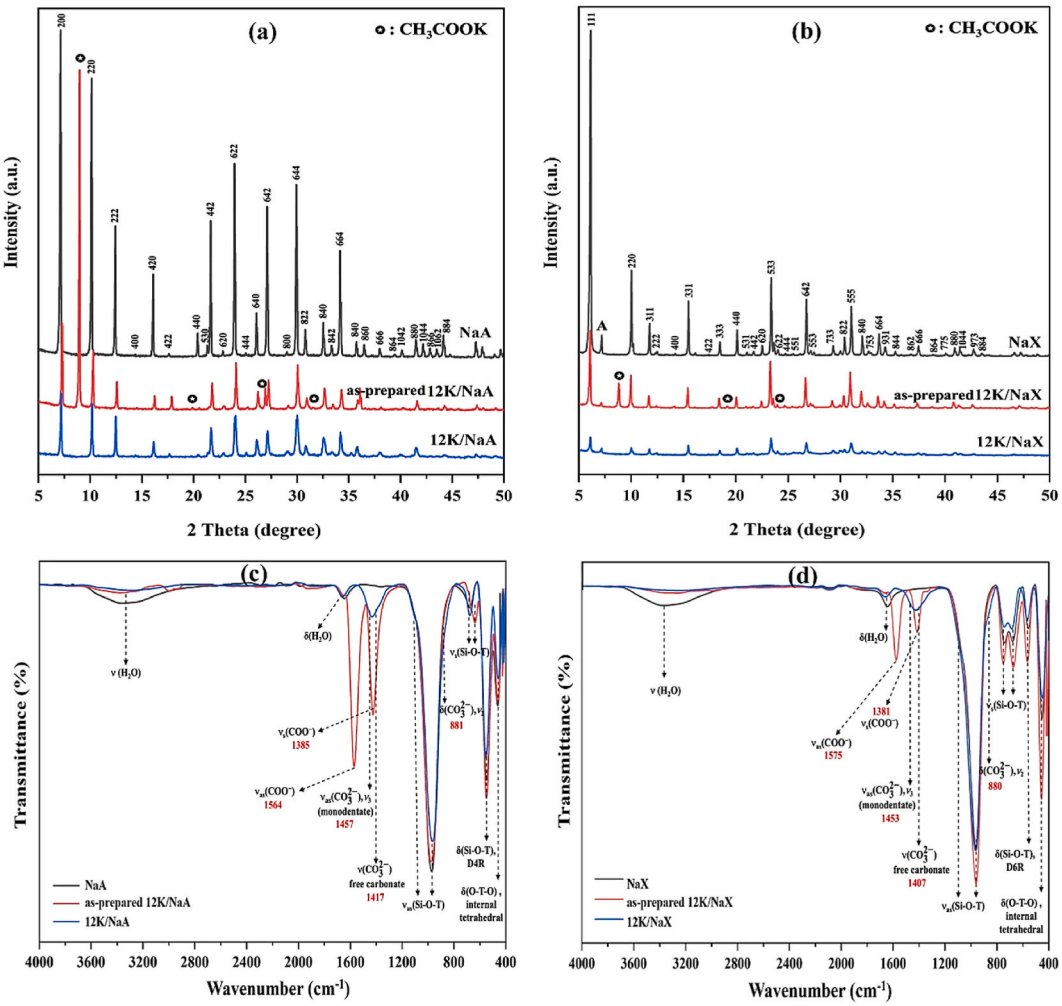

Fig. 3. (a,b) XRD pattern and (c,d) FTIR spectra of as-prepared and calcined 12K/NaA, and 12K/NaX compared to the bare zeolites.

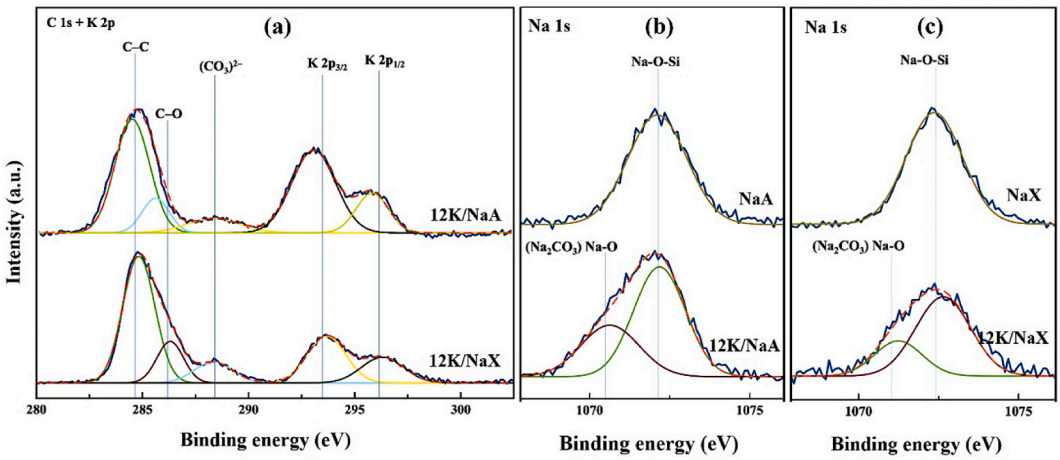

Fig. 4. XPS spectra of (a) C 1s + K 2p, (b and c) Na 1s in 12K/NaA and 12K/NaX.

profiles have been reported in the literature [4,27]. The total basicity of 12K/NaA and 12K/NaX were 1.204 and 1.189 mmol g^{-1}. The basicity of 12K/NaA was slightly higher than 12K/NaX, but the biodiesel yield was much higher. The difference in catalytic performance could be the influence of zeolite structure. Consequently, both catalysts were further characterized by other techniques.

Fig. 3a and b shows the XRD patterns of as-prepared and calcined 12K/NaA and 12K/NaX, respectively, compared with the bare zeolites. The zeolite peaks were indexed according to the simulated XRD pattern from the International Zeolite Association (IZA) [38]. The phase of commercial NaA is pure, whereas that of commercial NaX contains zeolite A as an impurity phase. The as-prepared catalysts show a similar pattern to the bare zeolite support but with lower peak intensities. The patterns also include peaks at 8.9, 14.3, and 27.2°, corresponding to potassium acetate precursors [4]. The acetate peaks from the as-prepared 12K/NaA are much stronger than those from as-prepared 12K/NaX, suggesting that 12K/NaA has potassium acetate on the external surface more than 12K/NaX. Kosawatthanakun et al. [4] reported that acetate peaks from 12K/NaX were more intense than those from 12K/NaY, implying more coverage on the external surface.

After calcination, the acetate peaks from both catalysts were no longer observed, suggesting that the precursor was transformed into other forms that are not detectable by XRD. Both catalysts still show characteristic peaks of the bare zeolites but with lower intensities. The decreased intensities could be from the lower crystallinity or the coverage of zeolite crystals by potassium species. It was suggested in the literature that the decrease in zeolite crystallinity is from the hydrolysis of Si–O–Al bonds, catalyzed by potassium during high-temperature treatment [3,4]. The decrease in peak intensities from 12K/NaA was much less than the 12K/NaX, suggesting that NaA is more stable than NaX upon the catalyst preparative conditions.

The FTIR spectra of the zeolites, as-prepared, and calcined catalysts are shown in Fig. 3c and d. The peaks corresponding to the functional groups of zeolite structures are as follows. The peaks at 464 cm^{-1} were assigned to internal tetrahedral TO_4 (T = Si or Al) bending vibration. The peaks at 551 cm^{-1} were assigned to the Si–O-T bending vibration of the double ring (D4R for NaA and D6R for NaX) [7,33]. The peaks at 756 cm^{-1} were attributed to symmetric stretching of Si–O-T and O–Al–O (Musyoka et al., 2015). The main asymmetric stretching of Si–O–Si was at 972, and 956 cm^{-1} for NaA and NaX [39].

The spectra of the as-prepared catalyst include peaks at 1434 cm^{-1} and 1564 cm^{-1} from symmetric and asymmetric stretching of COO^{-}, respectively [4,7]. These peaks from the as-prepared 12K/NaA are stronger than those from 12K/NaX. This observation suggests that potassium acetate disperses outside the cavity of NaA to a greater extent than 12K/NaX, consistent with the XRD results.

After calcination, the acetate peaks were not observed in both samples, and the peaks of the carbonate species emerged, indicating the transformation of potassium acetate to carbonate. The peaks at 881 cm^{-1} were assigned to out-of-plane bending (δ) of carbonate (ν_4 CO_3^{2-}). The peaks at 1087 and 1400 cm^{-1} were assigned to the symmetric stretching of carbonate (ν_1 CO_3^{2-}) and free carbonate species (ν CO_3^{2-}), respectively [40]. The peaks at 1450 cm^{-1} were assigned to the asymmetric stretching of carbonate (ν_3 CO_3^{2-}) or monodentate carbonate [41]. The carbonate peaks from 12K/NaA were stronger than those from 12K/NaX, confirming more carbonate on the external surface. Moreover, the bands corresponding to water were observed at 1650 cm^{-1} and 3200 cm^{-1} assigned to bending and symmetric stretching of –OH groups. The intensities of those bands in the as-prepared and calcined catalysts were lower than the bare zeolites due to the replacement of water in the zeolite cavities by potassium species, similar to the case of alumina reported by NolHakim et al. [27].

The XPS spectra of calcined 12K/NaA and 12K/NaX are presented in Fig. 4. The peaks of K $2p_{3/2}$ and K $2p_{1/2}$ from 12K/NaA are observed at 293.2 and 295.7 eV, respectively (Fig. 4a). Those peaks from 12K/NaX are at 293.8 and 296.3 eV [3,4,13]. Those peaks correspond to K_2CO_3. The lower binding energy from 12K/NaA indicates the weaker interaction between potassium and zeolite due to the greater amount on the external surface, consistent with the FTIR results.

The peaks of Na 1s from 12K/NaA and 12K/NaX are compared with the bare zeolites in Fig. 4b and c, respectively. The peak around 1072 eV corresponds to the charge-balancing sodium cation due to the interaction Na–O–Si [42,43]. The binding energy in 12K/NaA was slightly lower than 12K/NaX. The sodium peaks of calcined catalysts could be deconvoluted into two peaks. The peak around

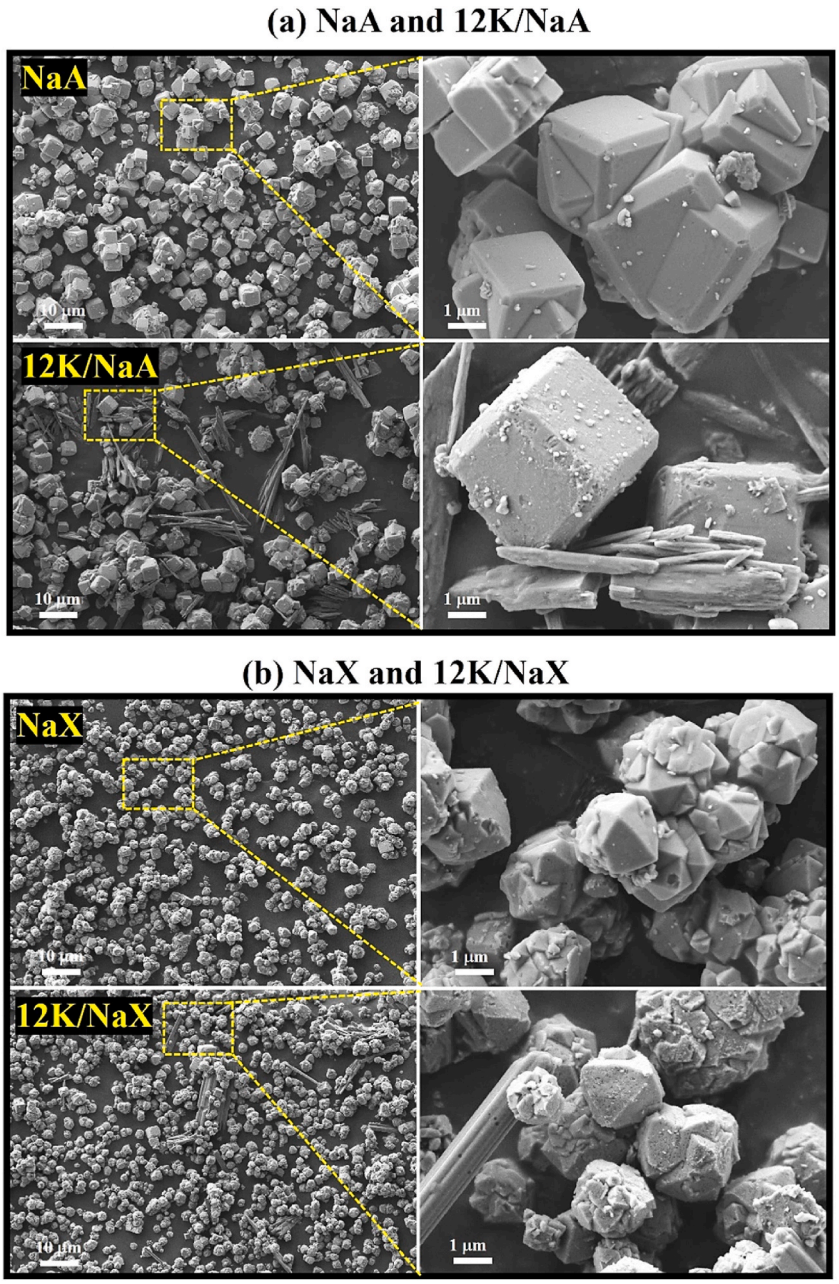

Fig. 5. SEM images of (a) NaA and 12K/NaA, (b) NaX and 12K/NaX with 1k and 10k magnification.

1071 eV corresponds to sodium carbonate [42]. The results confirm that sodium cation is exchanged with potassium to form carbonate species. By comparing the sodium peak, the sodium exchange on 12K/NaX was more than 12K/NaA.

The N_2 adsorption-desorption isotherms of bare zeolites and the zeolite-supported catalysts are shown inFig. S2 in Supplementary Materials. NaA and 12K/NaA do not adsorb N_2 because the zeolite pore size, 4 Å is smaller than the size of N_2 gas. Thus, this technique could not confirm the location of potassium species. In contrast, NaX and 12K/NaX have BET surface areas of 719 and 170 $m^2\ g^{-1}$, respectively. The decrease could be from the occupation of potassium or carbonate species in the zeolite cavities or the pore blockage or collapse of the zeolite structure [3,4]. The pore volumes of bare zeolites and calcined catalysts are shown in Table S3. The pore volume of 12K/NaX was 0.028 $cm^3\ g^{-1}$, which is larger than that of 12K/NaA. The results suggest that the pore volume might not significantly influence the activity of catalysts because the active species are on the external surface.

The TG curves of NaA, NaX, as-prepared 12K/NaA and 12K/NaA are shown in Fig. S3 in Supplementary Materials. The bare NaA and NaX show similar weight loss, but the NaX demonstrates that it is narrower and has more weight loss than the NaA. According to the Si/Al ratio of NaA (1.01) and NaX (1.21), the zeolite with a low Si/Al ratio is more hydrophilic and interacts with water more

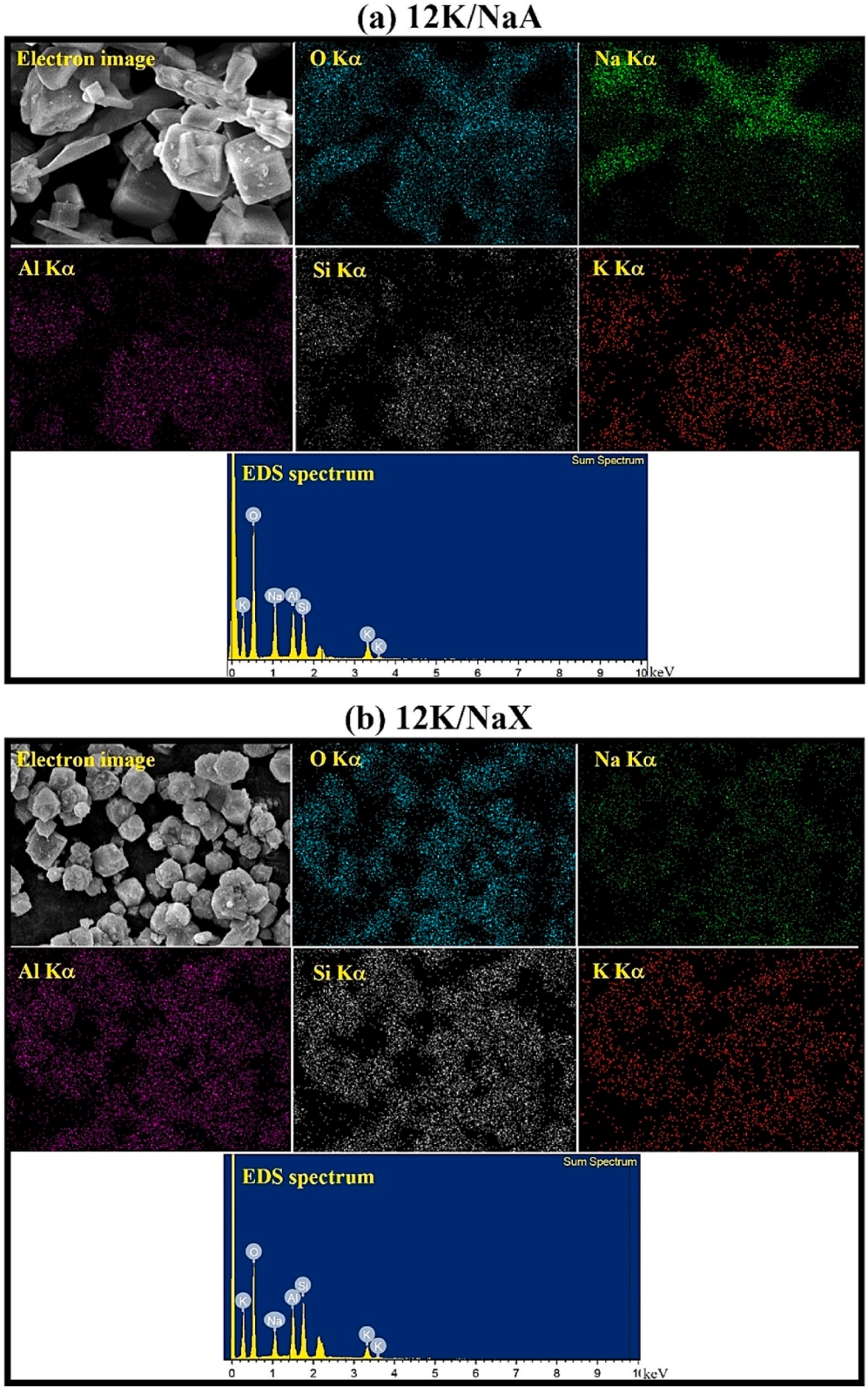

Fig. 6. EDS mapping of (a) 12K/NaA, and (b) 12K/NaX.

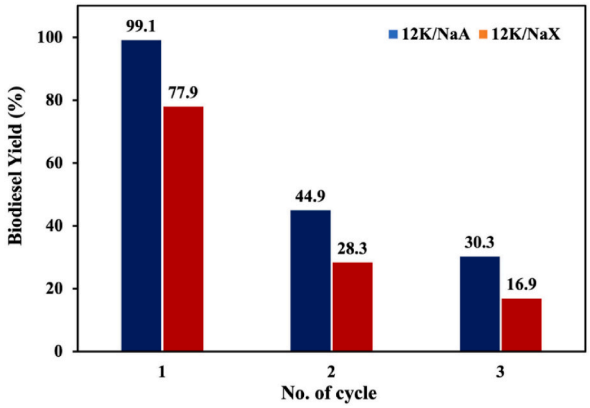

Fig. 7. Biodiesel yield from the repeated use of 12K/NaA and 12K/NaX catalysts in three reaction cycles.

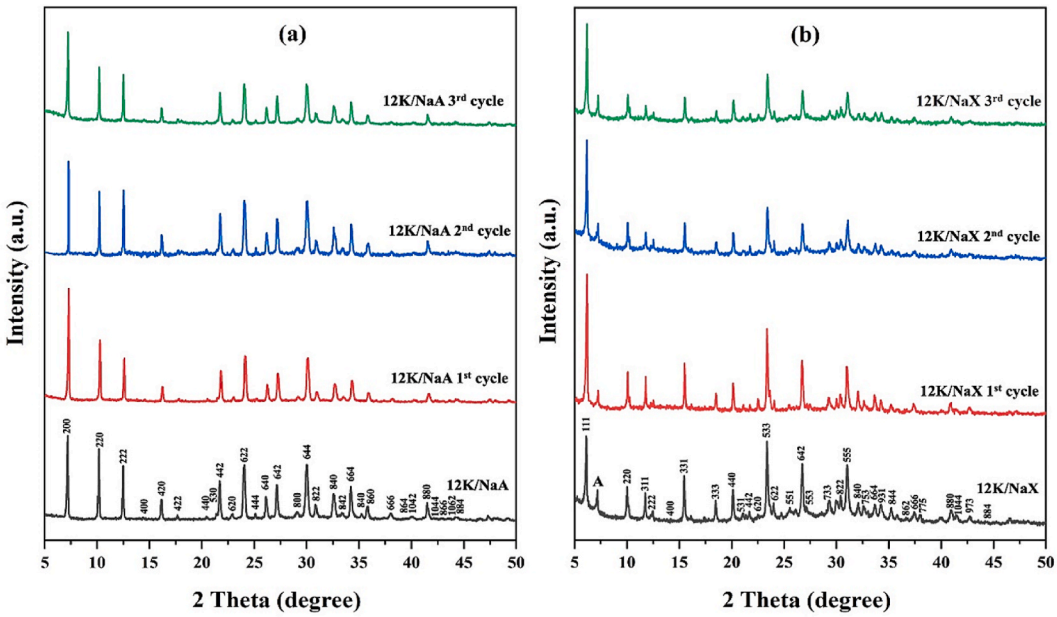

Fig. 8. XRD patterns of calcined and spent (a) 12K/NaA and (b) 12K/NaX catalysts from three reaction cycles.

strongly. The weight loss of as-prepared 12K/NaA and 12K/NaX are around 400 °C, corresponding to the decomposition of potassium acetate to carbonate [3,44,45]. Further weight loss occurs in both samples due to the decomposition of potassium carbonate to K_2O and CO_2 [27,46]. Based on these data, the suitable calcination temperature to convert potassium acetate to carbonate is 500 °C.

Fig. 5a and b shows SEM images of calcined 12K/NaA and 12K/NaX compared to their parent zeolites. The particles of NaA consist of single and polycrystals with cubic shapes and diameters around 2–4 μm. The calcined 12K/NaA has a morphology similar to the bare zeolite but with rough surfaces (Fig. 5a), probably from the coverage of potassium carbonate species. A similar zeolite morphology agrees with the XRD results, which show that the zeolite phase was retained after calcination. Moreover, the SEM image shows bundles of needle-shaped particles. Those needle-shaped particles could be either potassium or sodium carbonate. The needle morphology was reported in calcined catalysts prepared from the impregnation of KOH on zeolite NaA [26]. The difference from this work is that their zeolite completely collapses and becomes an amorphous phase. Our results confirm that the use of potassium acetate buffer precursor can prevent the zeolite structure from collapsing.

The SEM images of commercial NaX show polycrystal morphology with a particle diameter of around 1.5 μm. The images of calcined 12K/NaX (Fig. 5b) show a morphology similar to that of the parent zeolite. However, the zoom-in image showed spots of erosion on each crystal face. A similar observation was reported by Kosawatthanakun et al. [4]. The images of 12K/NaX also contain needle-shaped particles but with less quantity than those from 12K/NaA. To identify the elements in the needle-shaped particles, the calcined 12K/NaA and 12K/NaX were further analyzed by SEM-EDS.

The elemental mapping and EDS spectra of 12K/NaA are presented in Fig. 6a. Oxygen was observed on all particles because it is in

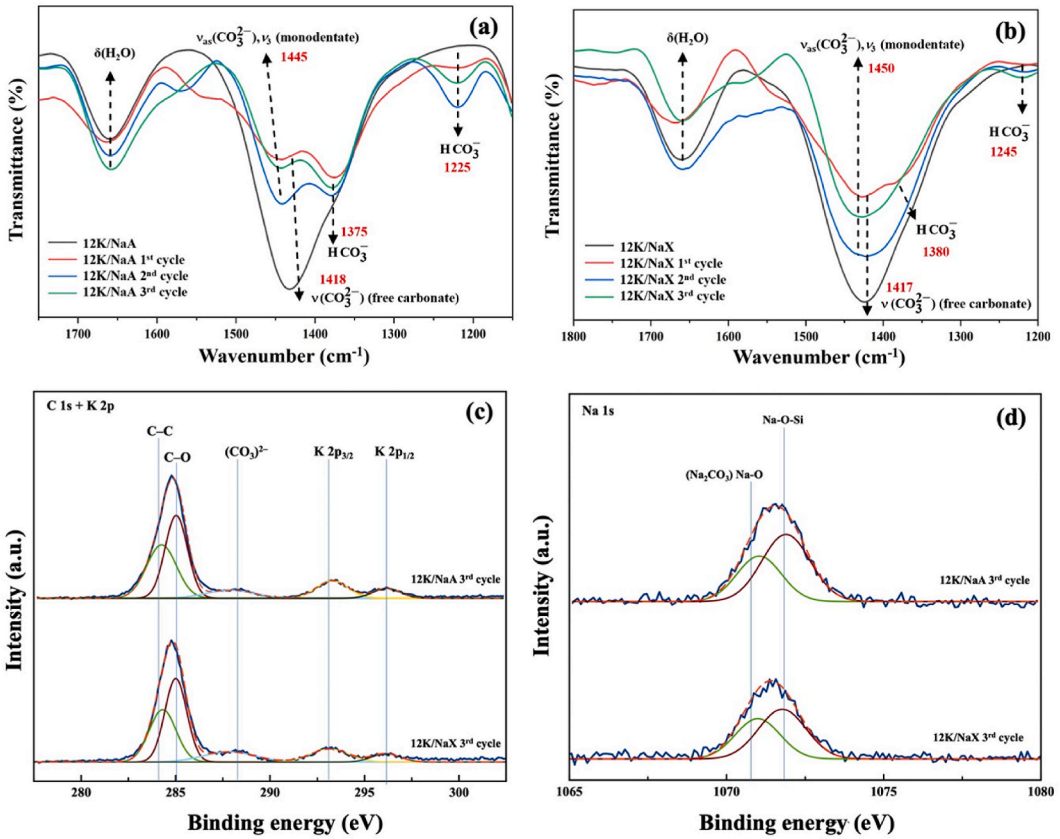

Fig. 9. (a,b) FTIR spectra of calcined and spent 12K/NaA and 12K/NaX catalysts, (c,d) XPS spectra of C 1s + K 2p and Na 1s from spent 12K/NaA and 12K/NaX catalysts after the third reaction cycle.

the zeolite structure and carbonate. Si and Al elements are distributed on the areas with cubic crystals, whereas Na is dispersed on needle-like particles and other non-cubic particles but not much on the zeolite cubic crystals. This observation suggests that the needle-like particles could be sodium carbonate. The distribution of potassium was also observed on cubic particles, but not on needle-like crystals suggesting that potassium species disperse on the surface of zeolite crystals and in the cavities. The elemental mapping of 12K/NaA suggests that sodium cation could exchange with potassium ion and become a counterion of carbonate. Potassium cation dispersed in the zeolite cavities and on external surfaces. The elemental mapping and EDS spectra of 12K/NaX are presented in Fig. 6b. All elements have similar distributions, suggesting that potassium cation dispersed on all particles and did not exchange much with sodium cation.

3.3. Catalyst reusability and stability

The biodiesel yields from three catalytic cycles on 12K/NaA and 12K/NaX are shown in Fig. 7. The yields from both catalysts were highest in the first run and decreased significantly in the following cycles. The yields from 12K/NaA were higher than those from 12K/NaX from all cycles. The decrease in biodiesel yield in the second run is the same as those from 12K/NaX and 12K/NaY reported in the literature [4]. Lower yields could be from the potassium leaching from the solid catalysts into the liquid products or changes in the catalyst physicochemical properties. Thus, the catalysts were further analyzed by ICP-OES, XRD, FTIR, XPS, and SEM-EDS.

The amount of potassium in the solid catalysts and liquid products (biodiesel and glycerol) determined by ICP-OES are listed in Table S4 in Supplementary Materials. The potassium leaching from 12K/NaA was 7.74 %, less than 12K/NaX which was 10.12 %. Potassium was not detected in the biodiesel product, but only found in glycerol, namely, 0.96 % from 12K/NaA and 1.24 % from 12K/NaX. Moreover, potassium species did not leach into methanol. Malins et al. [33] reported that K_2CO_3 partially dissolves in methanol and methanol/glycerol mixtures.

The XRD patterns of spent 12K/NaA and 12K/NaX catalysts are compared with the freshly calcined samples in Fig. 8. The spent catalysts from both entries have similar patterns to the calcined ones but with higher intensities. The potassium species covered on the surface of zeolite crystals could be removed by leaching, resulting in a better reflection of the X-ray beam.

The functional groups on the spent 12K/NaA and 12K/NaX catalysts are compared with the freshly calcined ones in Fig. 9a and b. The spectra are normalized and compared using the band ν_{as} (Si–O-T). The bands in the range 400–1200 cm^{-1} of the spent catalysts

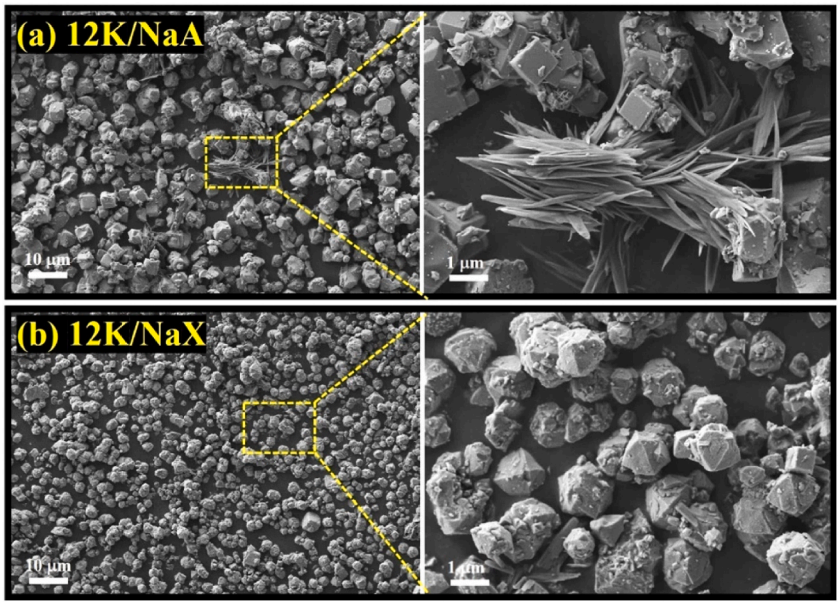

Fig. 10. SEM images of the catalyst after the third cycle biodiesel reaction: (a) 12K/NaA and (b) 12K/NaX with 1k and 10k magnification.

after the first to the third runs, corresponding to the functional groups of zeolites, were similar. The results suggest that both zeolites are stable through the cycles of catalytic testing.

The bands at the range 1200–1450 cm^{-1} of 12K/NaA, corresponding to carbonate species, show some differences after each run. From the spent catalysts, the free carbonate band at 1418 cm^{-1} decreased and the symmetric stretching of monodentate and bicarbonate species bands at 1385 and 1225 cm^{-1}, respectively, became more evident [41,47]. Moreover, the decreased intensity of free and asymmetric monodentate carbonate after the biodiesel reaction could result from the weak interaction of potassium with the zeolite supports. The carbonate species changes to bicarbonate which has lower basic strength and poorer catalytic activity [47–49]. In the case of 12K/NaX, the bands of free and monodentate carbonate decreased in the spent catalysts. The decrease was more evident than 12K/NaA. Moreover, the band of bicarbonate species from 12K/NaX was less evident than 12K/NaA. These results might be responsible for the greater decrease in the catalytic activity of 12K/NaX. The details of the full-range wavenumber at 400-4000 cm^{-1} are shown in Fig. S4 in Supplementary Materials.

The XPS spectra of spent 12K/NaA and 12K/NaX catalysts from the third run, including the binding energy of C 1s + K 2p and Na 1s are compared in Fig. 9c and d, respectively. The peaks of carbonate and potassium in both samples decreased from the fresh catalysts (see Fig. 4a), indicating that leaching occurs. In contrast, the peaks of sodium from the spent catalysts were similar to the fresh ones. The decrease in potassium and carbonate signals was consistent with the decrease in catalytic activity. Thus, the loss of activity could be the result of potassium and carbonate leaching.

The SEM images of the spent catalysts are shown in shown in Fig. 10. The morphology of the spent catalysts is similar to that of the fresh catalysts (see Fig. 6). The zeolite crystals and the needle-like particles in the spent catalysts are still observed. These results are consistent with the XRD patterns, showing that the zeolite crystallinity remained after the catalytic testing.

The elemental mapping and EDS spectrum of the spent 12K/NaA and 12K/NaX catalysts are shown in Fig. 11. The distribution of O, Na, Al, Si, and K are observed on all crystals, similar to the fresh catalysts. The mapping suggests that both sodium and potassium carbonate are present in the catalysts due to the partial solubility of both species in methanol and glycerol mixture, respectively.

4. Conclusions

Two catalysts containing 12 wt.% potassium supported on zeolite sodium A and X (12K/NaA and 12K/NaX) were prepared by ultrasound-assisted impregnation and compared in the transesterification of palm oil and methanol. Both zeolite structures are stable through catalyst preparation and testing. After calcination, the acetate precursor was converted to free and monodentate carbonate. 12K/NaA gives biodiesel yield of 99.1 ± 0.3 %, higher than 12K/NaX which was 77.9 ± 2.2 %. The difference arises from the location and form of carbonates. 12K/NaA has more carbonate on external surfaces and more monodentate carbonate than 12K/NaX. However, the potassium content decreased, and carbonate species were different after the catalytic testing. 12K/NaA has less potassium leaching, less change in carbonate form, and provides higher biodiesel yields in the second and third cycles than 12K/NaX. Consequently, 12K/NaA is a better catalyst than 12K/NaX.

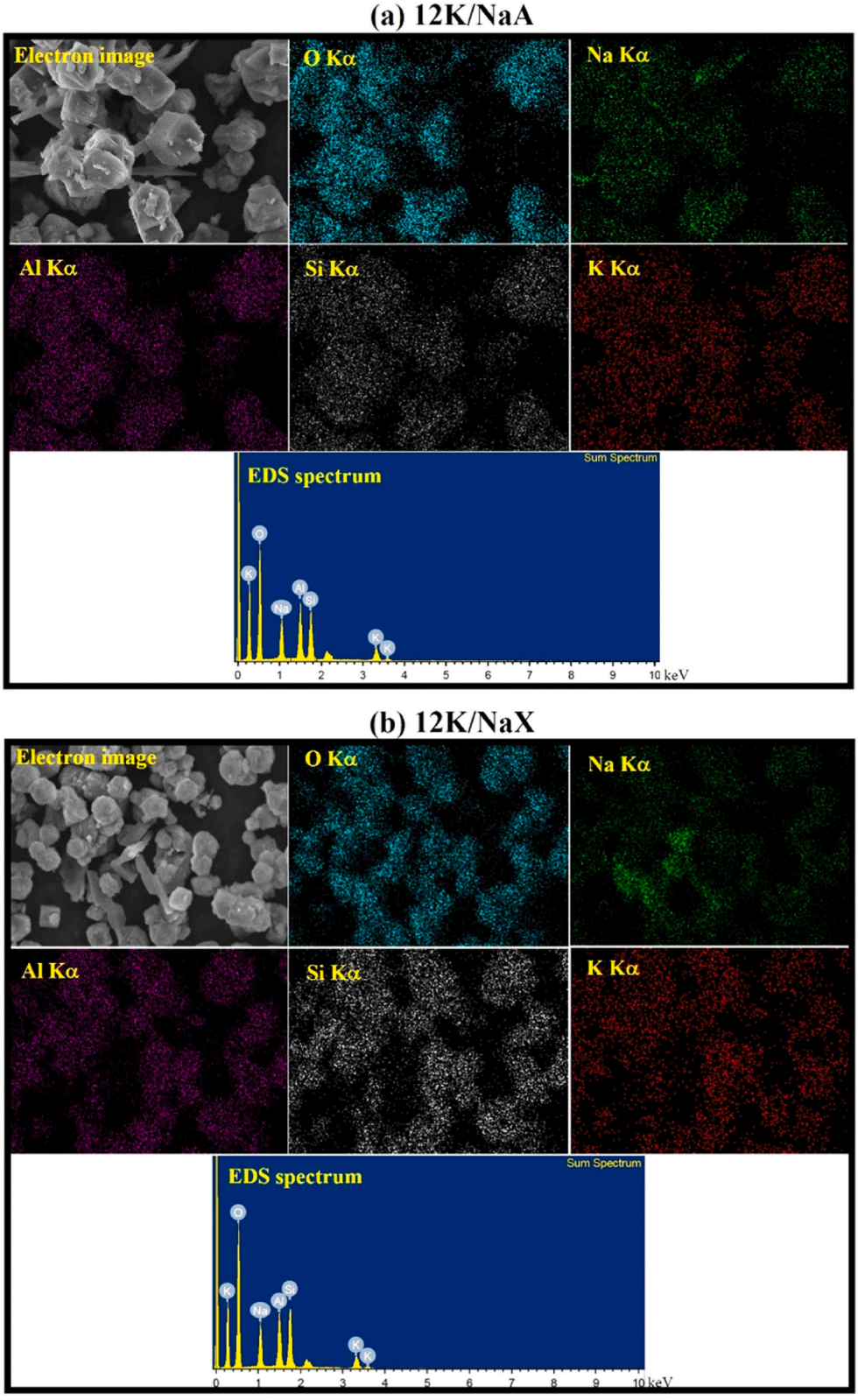

Fig. 11. SEM-EDS mapping and EDS spectrum of (a) reused 12K/NaA and (b)12K/NaX after the third reaction cycle.

CRediT authorship contribution statement

Piyanat Seejandee: Writing – review & editing, Writing – original draft, Visualization, Methodology, Investigation, Formal analysis, Data curation. **Nattawut Osakoo:** Supervision, Formal analysis. **Pakawan Sereerattanakorn:** Methodology, Formal analysis. **Panot Krukkratoke:** Methodology, Formal analysis. **Chalermpan Keawkumay:** Supervision, Formal analysis. **Chaianun Pansakdanon:**Methodology, Formal analysis. **Jatuporn Wittayakun:** Writing – review & editing, Writing – original draft, Validation, Supervision, Conceptualization. **Narong Chanlek:** Formal analysis. **Krittanun Deekamwong:** Methodology, Formal analysis. **Sanchai Prayoonpokarach:** Writing – review & editing, Writing – original draft, Validation, Supervision, Conceptualization.

Declaration of competing interest

The authors declare that they have no known competing financial interests or personal relationships that could have appeared to influence the work reported in this paper.

Acknowledgments

Scholarships for Piyanat Seejandee are from the Royal Golden Jubilee Ph.D. program supported by National Research Council of Thailand (NRCT) (Contact No. N41A661184) and Suranaree Univeristy of Technology. Scholarship for Chaianun Pansakdanon is from the Science Achievement Scholarship of Thailand (SAST). Full-time Doctoral Researcher Grant for Chalermpan Keawkumay, Nattawut Osakoo, and Krittanun Deekamwong was supported by (i) SUT, (ii) TSRI, and (iii) NSRF (90464/project code 90464), Thailand.

Appendix A. Supplementary data

Supplementary data to this article can be found online at https://doi.org/10.1016/j.heliyon.2024.e35975.

References

[1] M. Jayakumar, N. Karmegam, M.P. Gundupalli, K. Bizuneh Gebeyehu, B. Tessema Asfaw, S.W. Chang, et al., Heterogeneous base catalysts: synthesis and application for biodiesel production - a review, Bioresour. Technol. 331 (2021) 125054.
[2] A. Macario, G. Giordano, B. Onida, D. Cocina, A. Tagarelli, A.M. Giuffrè, Biodiesel production process by homogeneous/heterogeneous catalytic system using an acid–base catalyst, Appl. Catal. Gen. 378 (2010) 160–168.
[3] S. Rakmae, C. Keawkumay, N. Osakoo, K.D. Montalbo, R.L. de Leon, P. Kidkhunthod, et al., Realization of active species in potassium catalysts on zeolite NaY prepared by ultrasound-assisted impregnation with acetate buffer and improved performance in transesterification of palm oil, Fuel 184 (2016) 512–517.
[4] S. Kosawatthanakun, C. Pansakdanon, N. Sosa, N. Chanlek, F. Roessner, S. Prayoonpokarach, et al., Comparative properties of K/NaX and K/NaY from ultrasound-assisted impregnation and performance in transesterification of palm oil, ACS Omega 7 (2022) 9130–9141.
[5] S. Elfina, K. Pandiangan, N. Jamarun, F. Subriadi, H. Hafnimardiyanti, R. Roswita, Transesterification of palm oil catalyzed by CaO/SiO_2 prepared from limestone and rice husk silica, J. Multidiscip. Appl. Nat. Sci. 4 (2023).
[6] N. Supamathanon, J. Wittayakun, S. Prayoonpokarach, Properties of Jatropha seed oil from Northeastern Thailand and its transesterification catalyzed by potassium supported on NaY zeolite, J. Ind. Eng. Chem. 17 (2011) 182–185.
[7] S. Manadee, O. Sophiphun, N. Osakoo, N. Supamathanon, P. Kidkhunthod, N. Chanlek, et al., Identification of potassium phase in catalysts supported on zeolite NaX and performance in transesterification of Jatropha seed oil, Fuel Process. Technol. 156 (2017) 62–67.
[8] W. Xie, X. Huang, H. Li, Soybean oil methyl esters preparation using NaX zeolites loaded with KOH as a heterogeneous catalyst, Bioresour. Technol. 98 (2007) 936–939.
[9] I.B. Banković-Ilić, I.J. Stojković, O.S. Stamenković, V.B. Veljkovic, Y.-T. Hung, Waste animal fats as feedstocks for biodiesel production, Renew. Sustain. Energy Rev. 32 (2014) 238–254.
[10] Kumoro A. Cahyo, M.T.M.N. Saeed, Ultrasound-assisted transesterification of tropical goat fat – palm oil blend for biodiesel synthesis, Energy Convers. Manag. X 14 (2022) 100213.
[11] Chaiwat Sowcharoensuk, Industry Outlook 2024-2026 : Palm Oil Industry, Krungsri, Research, 2023.
[12] B. Thangaraj, P. Solomon, R. Srinivasan, L. Lin, Catalysis in biodiesel production-a review, Clean. Energy 3 (2018).
[13] N. Supamathanon, K. Boonserm, N. Osakoo, J. Wittayakun, S. Prayoonpokarach, N. Chanlek, et al., Potassium supported on zeolite-geopolymer hybrid materials as a new solid base catalyst for transesterification of soybean oil, Renew. Energy 202 (2023) 1460–1469.
[14] H. Wu, J. Zhang, Q. Wei, J. Zheng, J. Zhang, Transesterification of soybean oil to biodiesel using zeolite supported CaO as strong base catalysts, Fuel Process. Technol. 109 (2013) 13–18.
[15] C. Chen, S. Qu, M. Guo, J. Lu, W. Yi, R. Liu, et al., Waste limescale derived recyclable catalyst and soybean dregs oil for biodiesel production: analysis and optimization, Process Saf. Environ. Protect. 149 (2021) 465–475.
[16] A. Yusuff, M. Onibonoje, Biodiesel production from transesterified yellow grease by ZSM-5 zeolite-supported BaO catalyst: process optimization by Taguchi's experimental design approach, Mater. Renew. Sustain. Energy 12 (2023).
[17] S. Qu, C. Chen, M. Guo, J. Lu, W. Yi, J. Ding, et al., Synthesis of MgO/ZSM-5 catalyst and optimization of process parameters for clean production of biodiesel from Spirulina platensis, J. Clean. Prod. 276 (2020) 123382.
[18] T. Wang, X. Ma, N. Bingwa, H. Yu, Y. Wang, G. Li, et al., A novel bimetallic CaFe-MOF derivative for transesterification: catalytic performance, characterization, and stability, Energy 292 (2024) 130544.
[19] H. Li, Y. Wang, Z. Han, T. Wang, Y. Wang, C. Liu, et al., Nanosheet like CaO/C derived from Ca-BTC for biodiesel production assisted with microwave, Appl. Energy 326 (2022) 120045.
[20] G. Pampararo, D.P. Debecker, Sodium aluminate-catalyzed biodiesel synthesis, ACS Sustain. Chem. Eng. 11 (2023) 10413–10421.
[21] B.O. Yusuf, S.A. Oladepo, S.A. Ganiyu, Biodiesel production from waste cooking oil via β-zeolite-supported sulfated metal oxide catalyst systems, ACS Omega 8 (2023) 23720–23732.
[22] S.B.L. Ngomade, C.G. Fotsop, K.L.T. Nguena, I.K. Tchummegne, M.L.T. Ngueteu, A.K. Tamo, et al., Catalytic performances of CeO_2@SBA-15 as nanostructured material for biodiesel production from Podocarpus falcatus oil, Chem. Eng. Res. Des. 194 (2023) 789–800.

[23] M. Saad, B. Siyo, H. Alrakkad, Preparation and characterization of biodiesel from waste cooking oils using heterogeneous Catalyst (Cat.TS-7) based on natural zeolite, Heliyon 9 (2023) e15836.
[24] W. Greń, S.C. Parker, B. Slater, D.W. Lewis, Structure of zeolite A (LTA) surfaces and the zeolite A/water interface, J. Phys. Chem. C 114 (2010) 9739–9747.
[25] X. Zhang, D. Tang, M. Zhang, R. Yang, Synthesis of NaX zeolite: influence of crystallization time, temperature and batch molar ratio SiO2/Al2O3 on the particulate properties of zeolite crystals, Powder Technol. 235 (2013) 322–328.
[26] S. Trisupakitti, T. Phalama, P. Ponkham, W. Senajuk, P. Pimpanit, Biodiesel production from black acid oil using KOH/zeolite LTA catalyst, Koch Cha Sarn J. Sci. 42 (2018) 51–67.
[27] M. Lokman Nolhakim, Shohaimi N. Mohd, W.N.A. Wan Mokhtar, M.L. Ibrahim, R. Abdullah, Immobilization of potassium-based heterogeneous catalyst over alumina beads and powder support in the transesterification of waste cooking oil, Catalysts 11 (2021) 976.
[28] R. Foroutan, S.J. Peighambardoust, R. Mohammadi, S.H. Peighambardoust, B. Ramavandi, The potential of biochar derived from banana peel/Fe_3O_4/ZIF-67@K_2CO_3 as magnetic nanocatalyst for biodiesel production from waste cooking oils, Results Eng. 22 (2024) 102005.
[29] O.A. Mawlid, H.H. Abdelhady, M.G. Abd El-Moghny, A. Hamada, F. Abdelnaby, M. Kased, et al., Clean approach for catalytic biodiesel production from waste frying oil utilizing K_2CO_3/Orange peel derived hydrochar via RSM Optimization, J. Clean. Prod. 442 (2024) 140947.
[30] K. Montalbo, R. de Leon, O. Sophiphun, S. Manadee, S. Prayoonpokarach, J. Wittayakun, Characterization and catalytic performance of potassium loaded on rice husk silica and zeolite NaY for transesterification of Jatropha seed oil, Quim. Nova 36 (2013) 1116–1120.
[31] P. Khemthong, S. Prayoonpokarach, J. Wittayakun, Synthesis and characterization of zeolite LSX from rice husk silica, Suranaree J. Sci. Technol. 14 (2007) 367–379.
[32] S.M. Lee, N. Xu, J.R. Grace, A. Li, C.J. Lim, S.S. Kim, et al., Structure, stability and permeation properties of NaA zeolite membranes for H_2O/H_2 and CH_3OH/H_2 separations, J. Eur. Ceram. Soc. 38 (2018) 211–219.
[33] N.M. Musyoka, L.F. Petrik, E. Hums, A. Kuhnt, W. Schwieger, Thermal stability studies of zeolites A and X synthesized from South African coal fly ash, Rev. Chem. Intermed. 41 (2015) 575–582.
[34] A. Wang, P. Arora, D. Bernin, A. Kumar, K. Kamasamudram, L. Olsson, Investigation of the robust hydrothermal stability of Cu/LTA for NH_3-SCR reaction, Appl. Catal., B 246 (2019) 242–253.
[35] J. Poosumas, K. Ngaosuwan, A.T. Quitain, S. Assabumrungrat, Role of ultrasonic irradiation on transesterification of palm oil using calcium oxide as a solid base catalyst, Energy Convers. Manag. 120 (2016) 62–70.
[36] A.K. Mohammed, Z.A. Alkhafaje, I.M. Rashid, Heterogeneously catalyzed transesterification reaction using waste snail shell for biodiesel production, Heliyon 9 (2023) e17094.
[37] V. Indira, K. Abhitha, A review on recent developments in Zeolite A synthesis for improved carbon dioxide capture: implications for the water-energy nexus, Energy Nexus 7 (2022) 100095.
[38] M.M.J. Treacy, J.B. Higgins, Collection of Simulated XRD Powder Patterns for Zeolites Fifth (5th) Revised Edition. Collection of Simulated XRD Powder Patterns for Zeolites Fifth (5th) Revised Edition, 2007.
[39] V. Volli, M.K. Purkait, Selective preparation of zeolite X and A from flyash and its use as catalyst for biodiesel production, J. Hazard Mater. 297 (2015) 101–111.
[40] A. Cárdenas-Arenas, A. Quindimil, A. Davó-Quiñonero, E. Bailón-García, D. Lozano-Castelló, U. De-La-Torre, et al., Isotopic and in situ DRIFTS study of the CO_2 methanation mechanism using Ni/CeO_2 and Ni/Al_2O_3 catalysts, Appl. Catal., B 265 (2020) 118538.
[41] K. Coenen, F. Gallucci, B. Mezari, E. Hensen, M. van Sint Annaland, An in-situ IR study on the adsorption of CO_2 and H_2O on hydrotalcites, J. CO2 Util. 24 (2018) 228–239.
[42] B. Dong, Y. Xu, S. Lin, X. Dai, Characterizing and exploring the formation mechanism of salt deposition by reusing advanced-softened, silica-rich, oilfield-produced water (ASOW) in superheated steam pipeline, Sci. Rep. 5 (2015) 17274.
[43] W. Rongchapo, C. Keawkumay, N. Osakoo, K. Deekamwong, N. Chanlek, S. Prayoonpokarach, et al., Comprehension of paraquat adsorption on faujasite zeolite X and Y in sodium form, Adsorpt. Sci. Technol. 36 (2017) 026361741771539.
[44] C.E. White, J.L. Provis, L.E. Gordon, D.P. Riley, T. Proffen, J.S.J. van Deventer, Effect of temperature on the local structure of kaolinite intercalated with potassium acetate, Chem. Mater. 23 (2011) 188–199.
[45] M. Afzal, P.K. Butt, H. Ahmad, Kinetics of thermal decomposition of metal acetates, J. Therm. Anal. 37 (1991) 1015–1023.
[46] E.G. Silveira Junior, V.H. Perez, I. Reyero, A. Serrano-Lotina, O.R. Justo, Biodiesel production from heterogeneous catalysts based K_2CO_3 supported on extruded γ-Al_2O_3, Fuel 241 (2019) 311–318.
[47] A. Karelovic, P. Ruiz, Improving the hydrogenation function of Pd/γ-Al_2O_3 catalyst by Rh/γ-Al_2O_3 addition in CO_2 methanation at low temperature, ACS Catal. 3 (2013) 2799–2812.
[48] J.I. Di Cosimo, V.K. Díez, M. Xu, E. Iglesia, C.R. Apesteguía, Structure and surface and catalytic properties of Mg-Al basic oxides, J. Catal. 178 (1998) 499–510.
[49] C.I. Ezeh, M. Tomatis, X. Yang, J. He, C. Sun, Ultrasonic and hydrothermal mediated synthesis routes for functionalized Mg-Al LDH: comparison study on surface morphology, basic site strength, cyclic sorption efficiency and effectiveness, Ultrason. Sonochem. 40 (2018) 341–352.